이학석사학위논문

Stress drop scaling of the 2016 Gyeongju and 2017 Pohang seismic sequences using coda-based methods

코다파를 이용한 2016 경주와 2017 포항 지진 시퀀스의 응력강하 스케일링

February 2020

School of Earth and Environmental Sciences

Seoul National University

채 경 돈

Abstract

Two M5 earthquakes struck the southeastern Korean Peninsula in September 2016 and November 2017, causing damage near the epicentral areas. We analyze stress drop scaling of these two earthquake sequences using coda-based methods and Bayesian inversion. The 2016 Gyeongju earthquake sequence is a typical earthquake sequence generated by tectonic processes. In contrast, the 2017 Pohang earthquake sequence is believed to be related to fluid injections conducted for development of enhanced geothermal systems. As the two sequences occurred in the same tectonic regime, our study provides a good chance to compare stress drop scaling between a tectonic earthquake sequence and an earthquake sequence influenced by fluid injections. We found that the stress drops of events in the Pohang sequences are lower than those of the Gyeongju sequence with similar magnitude. Although it is likely that this difference results from focal depth variations, a reduction of stress drop due to fluid injections cannot be ruled out.

Keyword : coda spectral ratio, coda source calibration, corner frequency, stress drop, source scaling trend

Student Number : 2017-24073

Contents

Figure List

The symbols represent the mean value of site-corrected amplitude data with one standard deviation. Synthetic Brune curves (black lines) are the results of source calibration. The stars are the corner frequency on the Brune curve with the posterior distributions as a result of full Bayesian MCMC (Markov Chain Monte Carlo, MHS; Metropolis-Hastings Sampling method). We have recalculated the site-correction term of the Pohang sequence to overcome the significant discrepancies of f_c values (c).

7) Scaling relations of corner frequency and stress drop versus seismic moment for two earthquake sequences. (a) Constant Brune (1970; 1971) stress drop trends are represented by grey dotted lines. Black vertical and horizontal lines with the symbols represent one standard deviation. The source scaling trend of the Gyeongju sequence follows well with the previously reported trend (thick dotted lines) of coda-based source studies. Both source scaling trends cannot be explained by a constant stress drop model.

Table List

Chapter 1.

Introduction

Study of the scaling relationship between magnitude and stress drop for earthquakes occurring in a given region is important not only for understanding the basic physics of earthquakes but also for mitigating earthquake damage by precisely predicting earthquake ground motions of possible future earthquakes. There are many historical documents on the occurrence of large earthquakes (M > 6) in the southeastern part of the Korean Peninsula. However, the largest instrumentally recorded earthquake in this region is only M_L 5.8 (KMA; Korea Meteorological Administration). The possibility of larger earthquakes in this region exists. Efforts toward mitigating seismic risk in this region are very important because it has valuable infrastructure, including nuclear power plants and cities with dense populations. In this study, we analyze the stress drop scaling of two moderate earthquake sequences that occurred in the southeastern Korean Peninsula using analysis of coda waves, which is known to be more stable than analysis of direct waves (Mayeda et al., 2007; Yoo et al., 2010).

The two earthquake sequences considered in this study are the 2016 M_w 5.6 Gyeongju (GJ) earthquake and the 2017 M_w 5.5 Pohang (PH) earthquake sequences (Figures 1 and 2). The distance between the epicenters of the GJ and PH mainshocks is about 43 km, and both earthquakes occurred in the Gyeongsang Basin. The Gyeongsang Basin is a tectonic unit classified based on the tectonic evolution in the Korean Peninsula. Although the Pohang Basin, where the PH sequence occurred, had been tectonically active until recently compared to the epicentral region of the GJ sequence, the current tectonic environment for generating earthquakes in both regions should be similar because they belong to the same tectonic unit. We can also expect that tectonic stresses in both regions are similar because they are spatially close to each other. However, the reported source characteristic of the two sequences, especially the mainshocks, are quite different. The focal depth of the GJ mainshock is 14.5 km (Woo *et al.*, 2019a) and its focal mechanism determined by moment tensor inversion is strike slip. The PH mainshock occurred at a shallower depth (4.27 km; Lee *et al.*, 2019; Woo *et al.*, 2019b) and its faulting style is strike slip with a considerable thrust component. The most important difference between the two earthquakes is whether fluid injection affected the occurrence of earthquake.

The GJ mainshock is a natural earthquake generated due to tectonic stress, whereas the PH mainshock is a "runaway" earthquake triggered by the stress perturbation due to injecting fluids for the development of enhanced geothermal systems (EGS) (Ellsworth *et al.*, 2019). The objective of this study is to show that the different mechanisms between the tectonic and "runaway" earthquakes can be revealed by comparison of source parameters of the GJ and PH earthquake sequences, which occurred in the same tectonic regime.

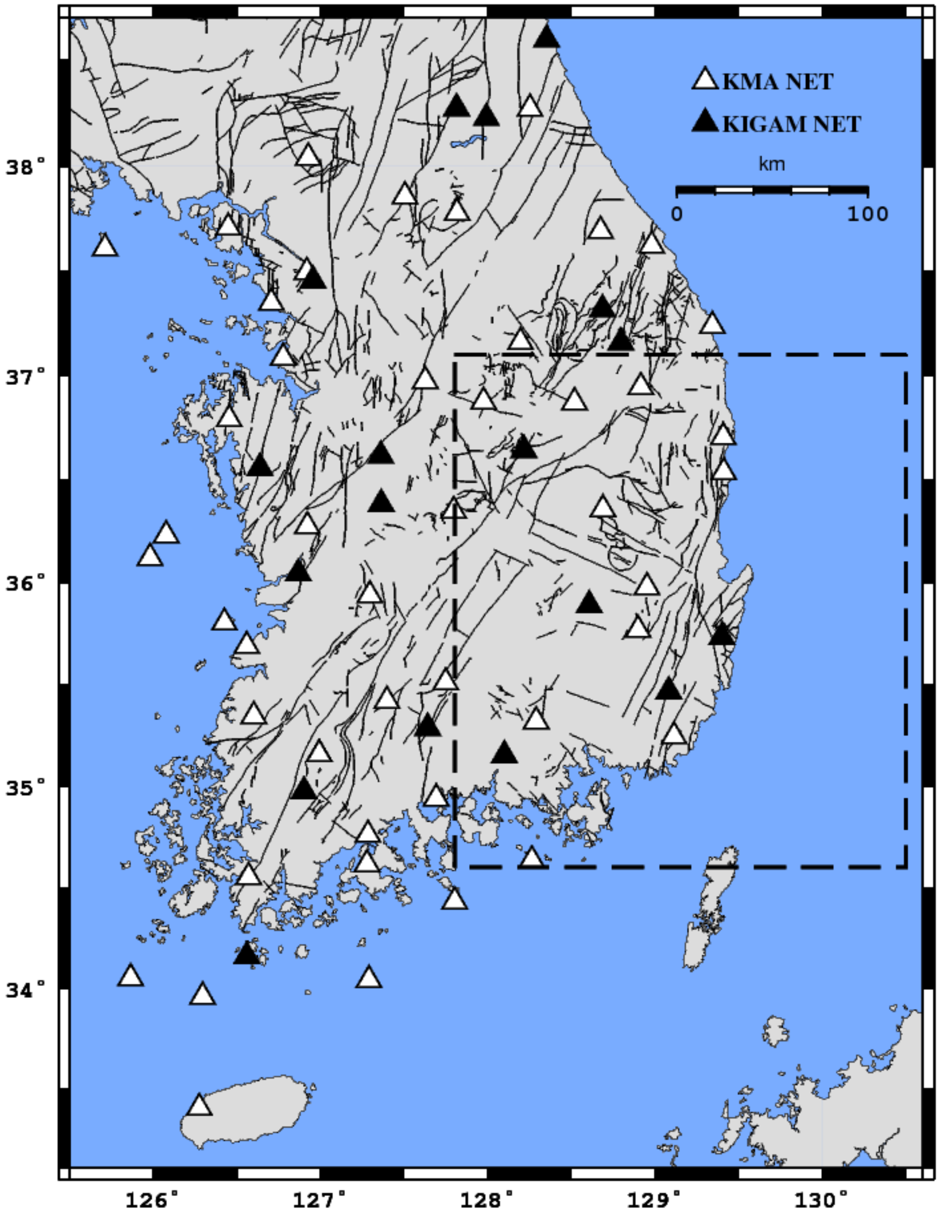

Figure 1. The Korea Meteorological Administration (KMA) network (white triangles) and Korea Institute of Geoscience and Mineral Resource (KIGAM) network (black triangles) were used to make synthetic coda envelope models and to perform the coda-based spectral ratio and source calibration study. The area in the dashed square is shown in Figure 2.

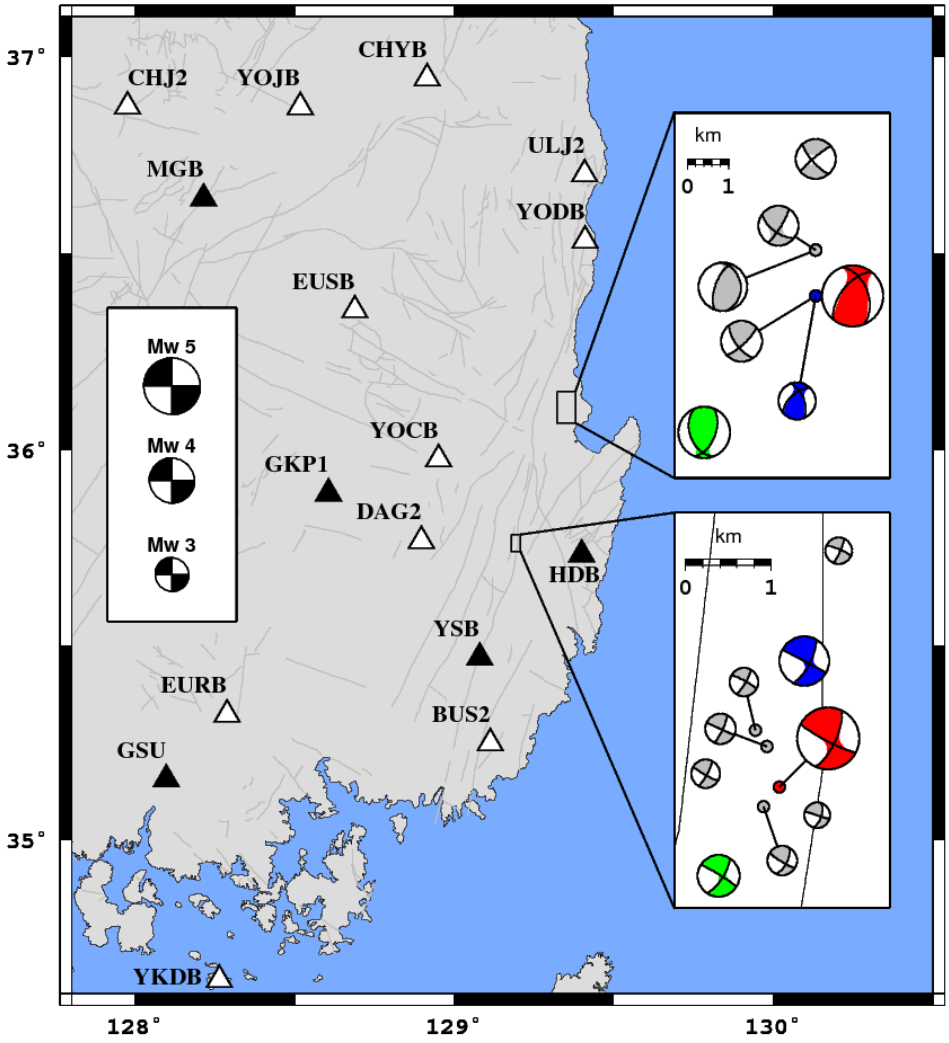

Figure 2. The study areas where the Gyeongju (right lower inset) and Pohang (right upper inset) earthquake sequences occurred. The focal mechanisms determined by ISOLA are plotted on the inset of each study area. Note that the Gyeongju sequence has only strike-slip faulting events but the Pohang sequence has reverse and strike-slip faulting events.

Chapter 2.

Data and Methods

Data used in this study are seismic waveforms recorded at broadband stations operated by the Korea Meteorological Administration (KMA) and the Korea Institute of Geoscience and Mineral Resources (KIGAM) (Figure 1), and they were divided into two sets for different research purposes. The first data set was used to define a reference coda envelope, which is necessary for calculating the source spectrum. For the lower frequency range (0.05–8.0 Hz), we used waveforms from earthquakes with magnitudes greater than 4.0 that occurred in and around the Korean Peninsula between 2006 and 2012. The sampling rate of this data set is 20 Hz. For the higher frequency range (8.0–14.0 Hz), we used waveforms from earthquakes in the 2016 Gyeongju sequence with magnitudes greater than 3.0; their sampling rate is 100 Hz. The second data set was used for analysis of source spectra for the GJ and PH sequences.

To determine a reference coda envelope, we defined its theoretical functional form following a previous study (Mayeda *et al.*, 2003) to be

$$E(t,f,r) = H\left(t - \frac{r}{v(f,r)}\right)\left(t - \frac{r}{v(f,r)}\right)^{-\gamma(f,r)} \times \exp\left[b(f,r)\left(t - \frac{r}{v(f,r)}\right)\right], \quad (1)$$

where *r*, *f*, and *t* indicate distance in km, frequency in Hz, and the time elapsed from the event origin time in s, respectively; *H* is the Heaviside step function; and $v(f,r)$ is the velocity of the peak arrival in km/s. Two functions, $b(f,r)$ and $\gamma(f,r)$, control the shape of the coda envelope. To define the reference coda envelope, we determined $v(f,r)$, $b(f,r)$, and $\gamma(f,r)$ from the observed data by following the procedures presented in Yoo *et al.* (2011). We defined reference coda envelopes for 14 consecutive narrow frequency bands (Table 1, Figure 3).

The relation between the observed and reference coda envelopes can be represented as follows:

$$A_C(t,f,r) = W_0(f)S(f)P(f,r)E(t,f,r), \tag{2}$$

where $A_C(t,f,r)$, $S(f)$, $P(f,r)$ and $W_0(f)$ are the observed coda envelope, site correction, path correction, and S-wave source amplitude, respectively.

To measure $A_C(t,f,r)$, we removed the instrument response of two horizontal component waveforms to velocity seismograms. Four-pole and two-pass Butterworth filters, of which corner frequencies correspond to 14 consecutive narrow frequency bands, were applied, and then an envelope for each frequency was calculated using

$$E_{\text{obs}} = \sqrt{v(t)^2 + h(t)^2}, \tag{3}$$

where $v(t)$ and $h(t)$ are the band-pass-filtered horizontal velocity seismogram and its Hilbert transform, respectively. To distinguish the observed and reference envelopes, we use E_{obs} for the observed envelope. The final observed envelope was calculated by taking the logarithm base 10 of two horizontal envelopes and then averaging them. By doing this, we measured $A_C(t,f,r)$ for each frequency and epicentral distance. We can see in Eq. (2) that changes in $A_C(t,f,r)$ with time for a given frequency and distance should be the same as the changes in $E(t,f,r)$. The difference between $A_C(t,f,r)$ and $E(t,f,r)$ is called non-dimensional coda amplitude (NDCA), and it can be measured by finding the optimum DC shift, which minimizes the L1 norm between $A_C(t,f,r)$ and $E(t,f,r)$. We then compared the reference and observed coda envelopes at each frequency band. Two methods are widely used to study seismic sources using measured NDCA. The first method involves directly estimating $W_0(f)$ by correcting $P(f,r)$ and $S(f)$ from NDCA. The advantage of this method is that it can be used to estimate source spectra of all events in a given region once models for $P(f,r)$ and $S(f)$ are defined. Because source spectra are available, we can estimate M_0 and f_c, the seismic moment in Nm and the corner frequency in Hz, which are two representative source parameters, but we can also estimate radiated energy. However, unless $P(f,r)$ and $S(f)$ are precise enough, the reliability of estimated source spectra can be low. The second method is to estimate f_c only, or f_c and M_0 together, from the ratio of NDCA between two events without calculating the individual source spectrum of each event (Mayeda *et al.*, 2007). This method is based on the assumption that if NDCAs are measured at the identical station and two earthquakes occurred at close locations, $P(f,r)$ and $S(f)$ for both events should be identical and the ratio of NDCA is the same as the ratio of the source spectra. In this case, we do not need to determine $P(f,r)$ and $S(f)$ to apply the method. However, this method is only applicable to event pairs with similar epicenters but large differences in magnitude. In this study, we are interested in studying source characteristics of two earthquake sequences and determining whether earthquakes in each sequence are spatially clustered. Therefore, a combined procedure of the two methods can be applied; the detailed procedure is as follows. First, we selected event pairs with a magnitude difference larger than 1 in each sequence. Total numbers of selected events and corresponding event pairs for the GJ sequence are 9 and 15, respectively, and 6 and 7 for the PH sequence. The maximum distance between epicenters among event pairs is 7 km. M_w for each event was independently calculated using ISOLA (Sokos and Zahradnik, 2008, Vackář *et al.*, 2017) software based on the waveform inversion method (Figure 2). We considered 66 stations for our analysis, but the actual number of data points used for each process was not consistent (Figure 1). To estimate f_c of both events from the spectral ratio for a given event pair, we used the Bayesian inversion method. The hierarchical scheme was applied to account for data error in the inversion (Bodin and Gass, 2003; Kim *et al.*, 2016). We assumed that prior probability of $\Delta\sigma$ is uniform in the range $10^{-3} - 10^{3}$ MPa. Once we selected $\Delta\sigma$, we calculated f_c by using the following equation, because M_0 of the event is pre-defined:

$$f_c = \frac{2.34\beta}{2\pi\left(\frac{7}{16}\cdot\frac{M_0}{\Delta\sigma}\right)^{\frac{1}{3}}}. \qquad (4)$$

Equation (4) was derived from the following two equations based on the circular fault model (Eshelby, 1957). Shear wave velocity (β) was set to be 3.5 km/s.

$$\Delta\sigma = \frac{7}{16}\frac{M_0}{r^3} \tag{5}$$

$$r = \frac{2.34\beta}{2\pi f_c}. \tag{6}$$

Using f_c and M_0 of both events, we can define a spectral ratio between two events based on Brune's source model as follows (Aki, 1967; Brune, 1970; 1971):

$$R(f) = \frac{M_{0_1}[1+(f/f_{c_2})^2]}{M_{0_2}[1+(f/f_{c_1})^2]}. \tag{7}$$

The misfit between the synthetic and observed spectral ratio was measured using the L1 norm and the likelihood function was defined as

$$L = \frac{1}{2\sigma} \times \exp\left[\sum_{i=1}^{n} \frac{|R_{\mathrm{syn}}(f_i) - R_{\mathrm{obs}}(f_i)|}{\sigma}\right], \tag{8}$$

where R_{syn} and R_{obs} indicate the synthetic and observed spectral ratio, respectively, and f_i represents the center frequency of a given frequency band. To consider data error in the inversion, we assumed that σ has uniform prior probability between 0 and 1. We updated model parameters (two stress drops and σ) 200,000 times using the Metropolis-Hastings sampling (MHS) method (Metropolis *et al.*, 1953; Hastings, 1970). After the first half of the calculations, which is considered a burn-in period, we selected 1 sample per every 100 calculations to estimate the posterior probability density (PPD) of two values of stress drop (or f_c) and σ. For each event pair, we selected the f_c

with highest PPD. The final f_c value for each event was calculated by averaging selected f_c values for all event pairs.

Final f_c values for only large events (M_w >= 4.0) were used for further analysis. The number of final f_c values was three for each of the PH and GJ sequences. Once we determined f_c and M_0, the theoretical Brune's source spectrum can be calculated using the following equation:

$$M(f) = \frac{M_0}{\left(1+\left(\frac{f}{f_c}\right)^2\right)}. \tag{9}$$

For each station, a site correction term can be determined by measuring the difference between the theoretical Brune's source spectrum and the corresponding NDCA. We note that a site correction term contains $P(f,r)$ and $S(f)$ in Eq. (1). Because we define the site correction terms of individual stations separately for PH and GJ sequences, we can ignore variation in the site correction term with distance. We calculated the difference between the theoretical Brune's spectrum and the NDCA for each event and then averaged them for each sequence to determine the final site correction term as a function of frequency. Once a site correction term was defined, we calculated the source spectrum for each event by correcting NDCA. By averaging the estimated source spectra of each event for all available stations, we calculated the final source spectrum for each event. To estimate the PPD of stress drop (or f_c) and M_w from the final source spectrum, we used Bayesian inversion, which is similar to the method previously applied for spectral ratio. We assumed that the stress drop and M_0 have uniform prior probability in the ranges between 10^{-3} and 10^{3} MPa and between –2 and 2 in logarithmic scale about the maximum value of the corrected NDCA, respectively. f_c was determined from a given stress drop and M_0. To consider data error, we adopted two parameters, σ_f^{rms} and σ_f^{SD}. Here σ_f^{rms} indicates an envelope fitting error when measuring coda amplitudes of observed envelopes at given frequency and σ_f^{SD} is defined as one standard deviation of the site-correction term at the given frequency. The likelihood function is defined as

$$L = \frac{1}{2} \times \exp\left[\sum_{i=1}^{n} \frac{|M_{\mathrm{syn}}(f_i) - M_{\mathrm{obs}}(f_i)|}{\sigma_f^{\mathrm{rms}} + \sigma_f^{\mathrm{SD}}}\right]. \quad (10)$$

The same sampling procedure of Bayesian inversion using the MHS method that was used for the spectral ratio method was applied to estimate the PPD of M_w and f_c. The PPD of stress drop was also determined from Eqs. (5) and (6). We can technically estimate source parameters of all events with measured NDCA. However, low signal-to-noise ratio of small events can distort the results. Therefore, we used 9 and 6 events with M_w larger than 3.0 for GJ and PH sequences, respectively. Because the number of available earthquakes in the PH sequence for the spectral ratio method to be applied to is insufficient, we recalculated the site correction term for three earthquakes in the PH sequence, which were used for determining the site correction term. We calculated Brune’s source spectrum using M_0 and f_c estimated by Bayesian inversion and used this spectrum to calculate a site correction term.

Frequency bands

No.	From	To	Center
FREQ01	0.05	0.1	0.075
FREQ02	0.1	0.2	0.15
FREQ03	0.2	0.3	0.25
FREQ04	0.3	0.5	0.4
FREQ05	0.5	0.7	0.6
FREQ06	0.7	1.0	0.85
FREQ07	1.0	1.5	1.25
FREQ08	1.5	2.0	1.75
FREQ09	2.0	3.0	2.5
FREQ10	3.0	4.0	3.5
FREQ11	4.0	6.0	5.0
FREQ12	6.0	8.0	7.0
FREQ13	8.0	11.0	9.5
FREQ14	11.0	14.0	12.5

Table 1. Frequency bands used for making coda envelopes.

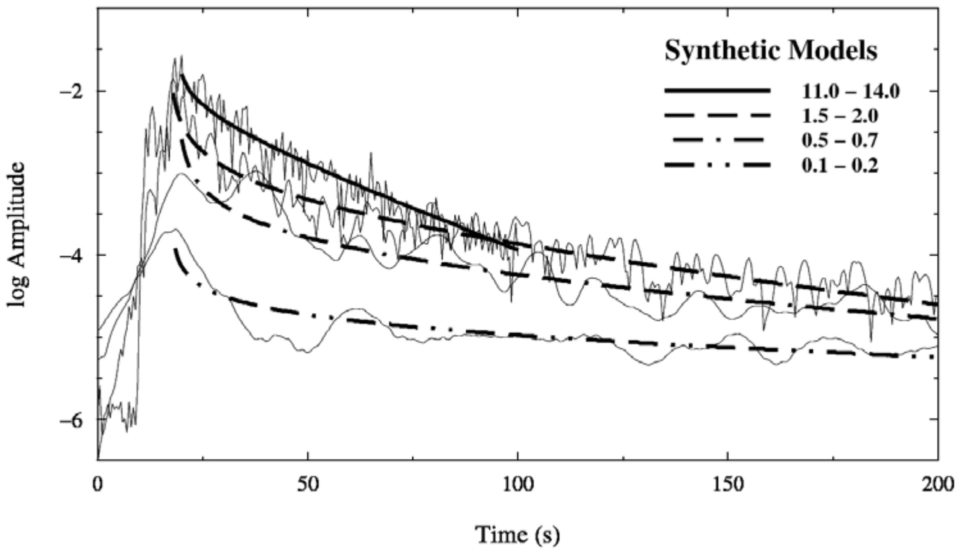

Figure 3. Narrow-band coda envelope of the Pohang main shock recorded at DAG2 station, showing the frequency-dependent decaying trends. Synthetic coda envelope models fit well with observed data envelopes (grey lines).

Chapter 3.

Results and Discussion

We applied coda-based methods and Bayesian inversion to the GJ and PH earthquake sequences. We calculated reference coda envelopes and compared them with observed coda envelopes. Figure 3 shows an example of comparison between the reference and observed coda envelopes at selected frequency bands. The final f_c value was calculated for each event using the MHS method and PPD was estimated; for each event pair, we selected the f_c with highest PPD. Figure 4 shows examples of spectral ratios determined for selected events. The calculated difference between the theoretical Brune's spectrum and the NDCA for each event was averaged for each sequence to determine the final site correction term as a function of frequency, as shown in Figure 5 for three events in the GJ sequence.

If the site correction term is well defined, we can expect that the estimated source spectra of events involved in determining site correction terms should be consistent with the site-corrected NDCA for the same event. In the case of the GJ sequence, we can see that the two values are well matched, as expected (Figure 6(a)). However, there are significant discrepancies in the PH sequence (Figure 6(c)). The reason for these discrepancies appears to be that original estimates of f_c from the spectral ratio method for the PH sequence are not proper because the number of applicable earthquakes is insufficient. To overcome this problem, we recalculated the site correction term for three earthquakes in the PH sequence, which were used for determining the site correction term (Figure 6(b)). The corrected NDCA using the recalculated site correction term shows a significantly improved fit to the theoretical Brune's spectrum (Figure 6).

Using coda-based methods and Bayesian inversion, we estimated PPD of M_w, f_c, and stress drop for 12 and 7 earthquakes in the GJ and PH sequences, respectively (Table 2). Stress drop scaling for both the GJ and PH sequences show that stress drop increases with increasing magnitude in overall scale (Figure 7). It is interpreted as the result that cannot be explained by the classic self-similar model with constant stress drop (Aki, 1967). Estimates of stress drop appear to be very scattered for smaller earthquakes (M_w < ~3.5) in both sequences. This may indicate that estimates of stress drop for smaller events are not stable because of low signal-to-noise ratio. One thing to note is that the stress drop of the smallest PH event (PH01 in Table 2) is much smaller than that of other events with similar magnitudes. For relatively larger events (M_w >= 4.0) in the GJ sequence, it is likely that stress drop increases with increasing M_w in a range between M_w 4.5 and 5.5. This observation is consistent with other previous studies using similar coda-based methods (Mayeda and Malagnini, 2009; Malagnini *et al.*, 2010; Yoo *et al.*, 2010; Yoo and Mayeda, 2013). For the PH sequence, we cannot see the increasing trend in the given magnitude range because the stress drop of the PH mainshock (PH02) is smaller than those of ones with similar magnitudes in the GJ sequence. In addition, stress drops of two other PH events (PH04 and PH07) with M_w larger than 4.0 are also smaller than stress drops of similar sized GJ events.

To summarize the characteristics of stress drop scaling for the two sequences, stress drops of the PH sequence appear to be smaller than those of the GJ sequence and two PH events (PH01 and PH02) have much smaller stress drops compared with those of events with similar magnitudes in the GJ sequence. The stress drop of PH01 (M_w 3.3) is smaller than that of GJ13 (M_w 3.3) by a factor of about 4. The stress drop of PH02 (M_w 5.5) is smaller than that of GJ03 (M_w 5.6) and GJ01 (M_w 5.1) by a factor of 4.3 and 2.5, respectively. Estimates of the stress drops for the GJ and PH mainshocks reported by other studies show similar results. Son *et al.* (2018) reported that the stress drop of GJ03 is 11.2 MPa by using analysis of the S-wave source spectrum. The mean stress drop of the same event derived from finite fault inversion using the empirical Green's function method is 23 MPa (Uchide and Song, 2018). These values are somewhat larger than our estimate (8.29 MPa). For PH02, Song and Lee (2019) estimated the mean stress drop of PH02 to be about 2 MPa from finite fault inversion using InSAR data, and this value is consistent with our result (1.92 MPa). We note that PH02 and PH01 are considered anthropogenic earthquakes (Kim *et al.*, 2018; Grigoli *et al.*, 2018; Lee *et al.*, 2019; Ellsworth *et al.*, 2019; Woo *et al.*, 2019b). PH01 is an induced earthquake, which occurred during a period when fluid injections for EGS development were conducted. PH02 (the PH mainshock) is considered a "runaway" earthquake. It means that its occurrence is affected by fluid injections even though it released strain energy accumulated through natural tectonic processes (Ellsworth *et al.*, 2019). Therefore, we can raise the question whether the low stress drops of PH02 and PH01 result from the influence of fluid injections. There have been several studies reporting that stress drops of induced earthquakes are smaller than those of tectonic earthquakes (Sumy *et al.*, 2017; Boyd *et al.*, 2017; Hough, 2014). Hough (2014) argued that stress drops of induced earthquakes are smaller than those of tectonic earthquakes by a factor of 2–10 based on differences in intensity between tectonic and induced earthquakes measured by a “Did You Feel It?” system. Although the stress drop difference between the PH and GJ mainshocks derived in this study lies within the range proposed by Hough (2014), it is not enough to conclude that the low stress drops observed in the PH sequence, especially for PH02 and PH01, are caused by fluid injections. It is well known that stress drop is controlled by many other factors, such as focal depth, faulting type, and heat flow. Therefore, it is possible that discrepancy in stress drop can be attributed to other factors. The PH and GJ mainshocks differ in several ways besides fluid injection. First, the focal depth of the PH mainshock (4.27 km; Lee *et al.*, 2019) is much shallower than that of the GJ mainshock (14.5 km; Woo *et al.*, 2019a). Second, whereas the faulting type of the GJ mainshock is nearly pure strike-slip, the PH mainshock is strike slip with considerable thrust-faulting components.

Although several studies have found that there is no clear depth dependence of stress drop (Wu *et al.*, 2018; Allmann and Shearer, 2009), most previous studies support the theory that shallow earthquakes have lower stress drops than deep earthquakes (Huang *et al.*, 2017; Oth, 2013). Huang *et al.* (2017) reported that induced earthquakes with deep focal depths (< 5 km) show similar stress drops as tectonic earthquakes in the central United States and concluded that induced and tectonic earthquakes are not distinguishable based only on differences in stress drop. Therefore, it is possible that the lower stress drop of the PH mainshock compared to the GJ mainshock is caused only by the difference in focal depth. Difference in focal depth can explain why stress drops of PH events are relatively lower than those of GJ events. However, it is still not clear why two events in the PH sequence, which are likely to be influenced by fluid injections, have much lower stress drops. Regarding the faulting style of earthquakes, the relations between faulting style and stress drop reported by previous studies are not consistent. In general, it is well accepted that reverse-faulting earthquakes have higher stress drop (e.g., McGarr, 1984; McGarr and Fletcher, 2002). However, Allmann and Shearer (2009) suggested that stress drop of strike-slip is higher than that of other faulting types. Our observation shows that stress drop of the GJ mainshock, which has pure strike-slip mechanism, is higher than that of the PH mainshock, which has considerable reverse-faulting components; this is consistent with the result of Allmann and Shearer (2009). Oth (2013) suggested that stress drop variations are strongly correlated with heat flow variations in crustal earthquakes in Japan. Therefore, heat flows can be another factor that affects stress drop, but we don't have enough information on whether there is a considerable difference in heat flow between the epicentral regions of the GJ and PH sequences.

2016 Gyeongju & 2017 Pohang

Event (No.)	Lat	Lon	Dep	Mw1	Mw2	fc1 (Hz)	fc2 (Hz)	Δσ1 (MPa)	Δσ2 (MPa)
2016.256.104432 (GJ01)	35.77	129.20	14.96	5.14	5.13	0.7067 ± (0.0254)	0.7314 ± (0.0040)	4.7304 ± (0.0762)	4.7476 ± (0.0089)
2016.256.111050 (GJ02)	35.76	129.19	15.83		3.19		3.2319 ± (0.0129)		0.5058 ± (0.0275)
2016.256.113254 (GJ03)	35.75	129.19	14.46	5.57	5.58	0.5695 ± (0.0210)	0.5214 ± (0.0049)	10.552 ± (0.0630)	8.2693 ± (0.0112)
2016.256.141827 (GJ04)	35.78	129.20	13.83	3.07	3.14	2.7905 ± (0.0281)	2.9147 ± (0.0108)	0.2646 ± (0.0845)	0.3179 ± (0.0236)
2016.256.145230 (GJ05)	35.76	129.19	13.52	3.21	3.26	3.7296 ± (0.0396)	2.5540 ± (0.0363)	0.9833 ± (0.1189)	0.3178 ± (0.0848)
2016.256.153710 (GJ06)	35.78	129.21	13.53		3.07		4.7058 ± (0.0128)		1.0508 ± (0.0288)
2016.256.232447 (GJ07)	35.76	129.18	13.00	3.23	3.25	4.3384 ± (0.0322)	3.9294 ± (0.0112)	1.6544 ± (0.0967)	1.1465 ± (0.0270)
2016.257.053142 (GJ08)	35.76	129.19	13.96		3.03		3.8057 ± (0.0134)		0.4737 ± (0.0293)
2016.263.113358 (GJ09)	35.75	129.18	15.80	4.46	4.49	1.1497 ± (0.0299)	1.2219 ± (0.0085)	1.964 ± (0.0897)	2.4671 ± (0.0198)
2016.265.025354 (GJ10)	35.76	129.19	13.79	3.43	3.42	4.8447 ± (0.0285)	4.4477 ± (0.0114)	4.3795 ± (0.0856)	2.9518 ± (0.0286)
2016.272.073430 (GJ11)	35.76	129.19	12.96		3.14		3.6272 ± (0.0150)		0.6046 ± (0.0333)
2016.276.115307 (GJ12)	35.75	129.20	15.42	2.98	2.94	6.4122 ± (0.0321)	5.4063 ± (0.0137)	2.1402 ± (0.0966)	1.0114 ± (0.0324)
2016.284.135910 (GJ13)	35.75	129.19	14.40	3.3	3.31	3.0970 ± (0.0336)	2.8868 ± (0.0119)	0.9671 ± (0.1011)	0.5456 ± (0.0257)
2017.105.023113 (PH01)	36.11	129.36	5.0	3.33	3.34	2.7547 ± (0.0545)	1.7951 ± (0.0255)	0.7291 ± (0.1645)	0.1381 ± (0.0517)
2017.319.052931 (PH02)	36.11	129.37	5.0	5.48	5.44	0.3441 ± (0.0258)	0.3759 ± (0.0086)	1.728 ± (0.0776)	1.9231 ± (0.0128)
2017.319.060949 (PH03)	36.09	129.34	8.0(KMA)		3.45		3.1046 ± (0.0452)		0.8943 ± (0.0914)
2017.319.074930 (PH04)	36.12	129.36	6.6	4.31	4.3	1.039 ± (0.0235)	1.3103 ± (0.0065)	0.8138 ± (0.0706)	1.6627 ± (0.0117)
2017.323.144547 (PH05)	36.12	129.36	4.2	3.53	3.54	3.6647 ± (0.0448)	2.6094 ± (0.0182)	2.778 ± (0.1346)	0.9029 ± (0.0404)
2017.323.210515 (PH06)	36.14	129.36	4.0	3.59	3.62	2.9533 ± (0.0272)	2.1699 ± (0.0166)	1.8601 ± (0.0817)	0.6295 ± (0.0301)
2018.041.200303 (PH07)	36.08	129.33	8.0	4.61	4.6	1.2172 ± (0.0372)	0.7664 ± (0.0058)	3.8628 ± (0.1123)	1.0808 ± (0.0114)

Table 2. Source parameters of the 2016 Gyeongju and 2017 Pohang earthquake sequences by (1) coda-based spectral ratio and (2) source calibration methods. (*hypoDD relocation data from Woo *et al.* (2019b) data were used for Gyeongju, and Pohang sequence location data from the KMA catalog and focal depths were computed by ISOLA.)

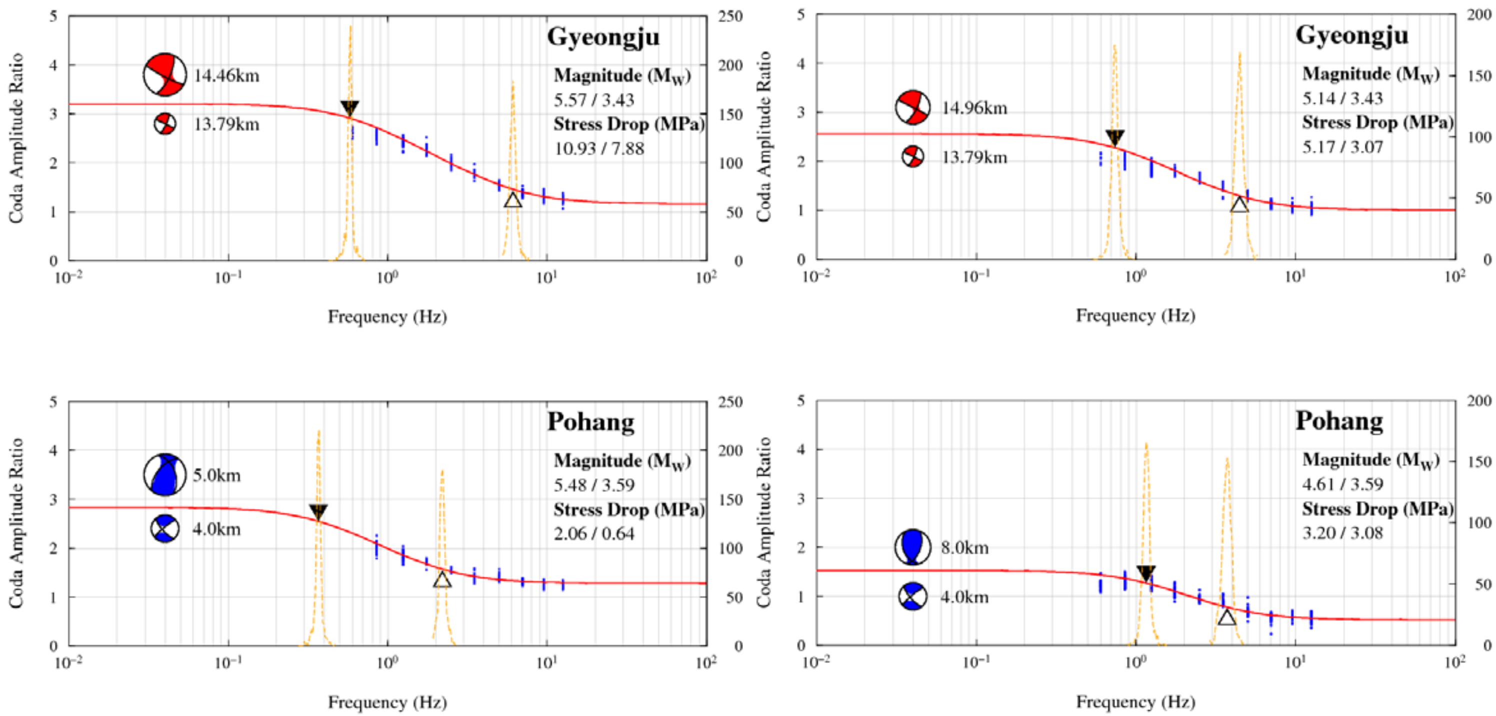

Figure 4. The spectral ratio of Gyeongju (red) main and foreshocks and Pohang (blue) main and aftershock with the same EGF events in sequence. Focal mechanisms are determined by ISOLA, and the Gyeongju events depth information is taken from Woo et al. (2019b) and Pohang events depths from ISOLA. Yellow dashed graphs show that use of posterior distribution to determine corner frequency by full-Bayesian MCMC. The two colors of triangles indicate the corner frequencies of target and EGF events.

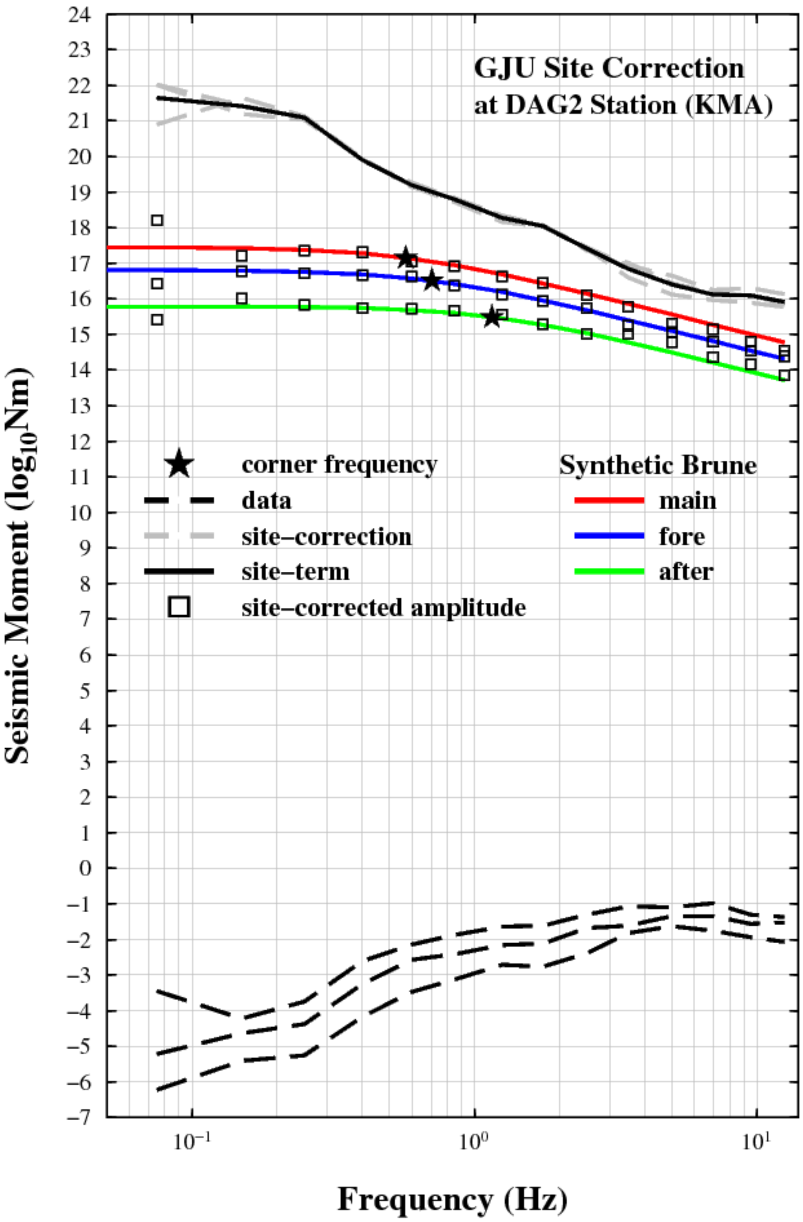

Figure 5. The calculated site correction term (black line) of GJ fore (M_w 5.13), main (M_w 5.58), and largest aftershock (M_w 4.49) at DAG2 station. We made the synthetic Brune model (colored lines) for events. By subtracting the observed amplitude (black dotted lines) from the synthetic model, we determined the correction term (grey dotted lines) for each event. The site correction term of this station is made by averaging all correction terms. With the site correction term of the station, we can apply site correction to every recorded event amplitude.

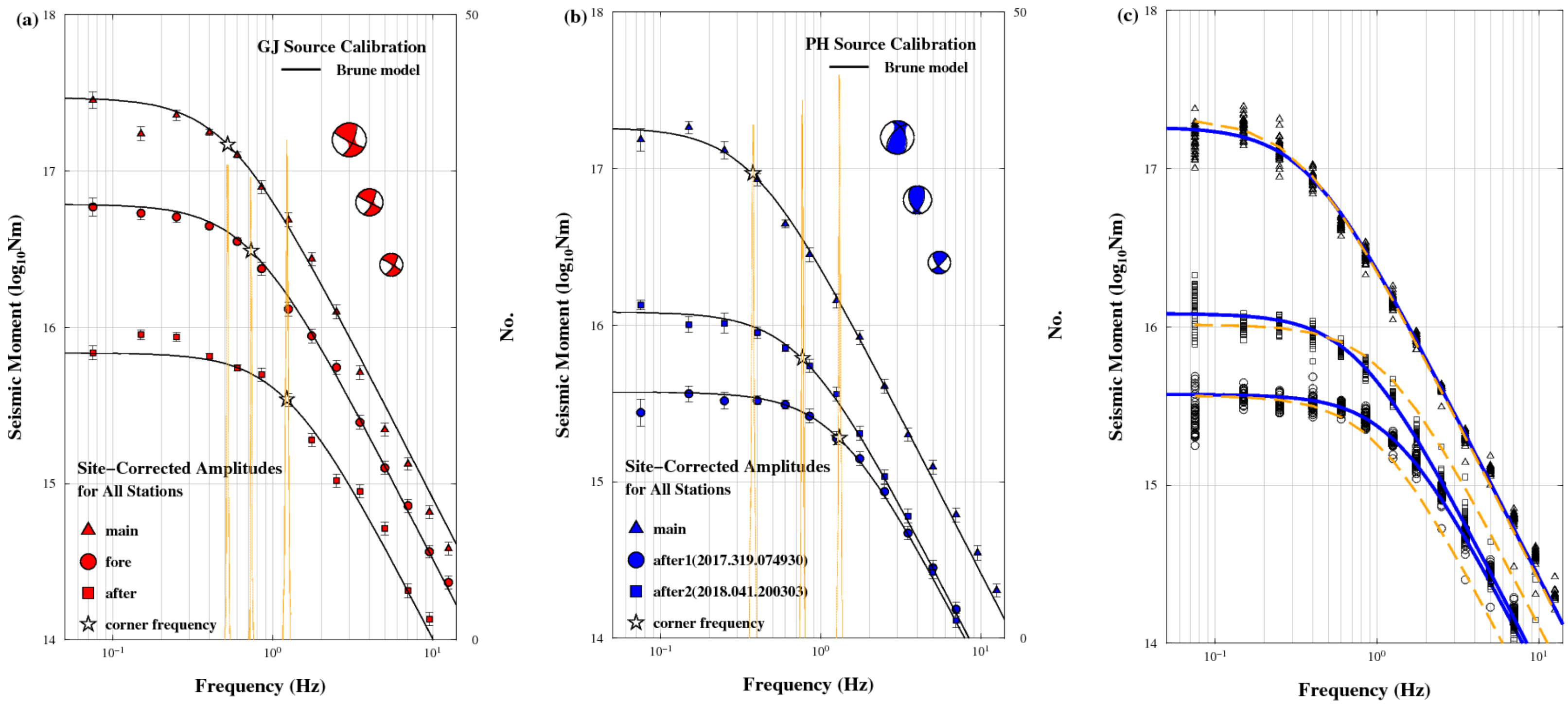

Figure 6. Source calibration results of two earthquake sequences, (a) Gyeongju and (b-c) Pohang. The symbols represent the mean value of site-corrected amplitude data with one standard deviation. Synthetic Brune curves (black lines) are the results of source calibration. The stars are the corner frequency on the Brune curve with the posterior distributions as a result of full Bayesian MCMC (Markov Chain Monte Carlo, MHS; Metropolis-Hastings Sampling method). We have recalculated the site-correction term of the Pohang sequence to overcome the significant discrepancies of f_c values (b).

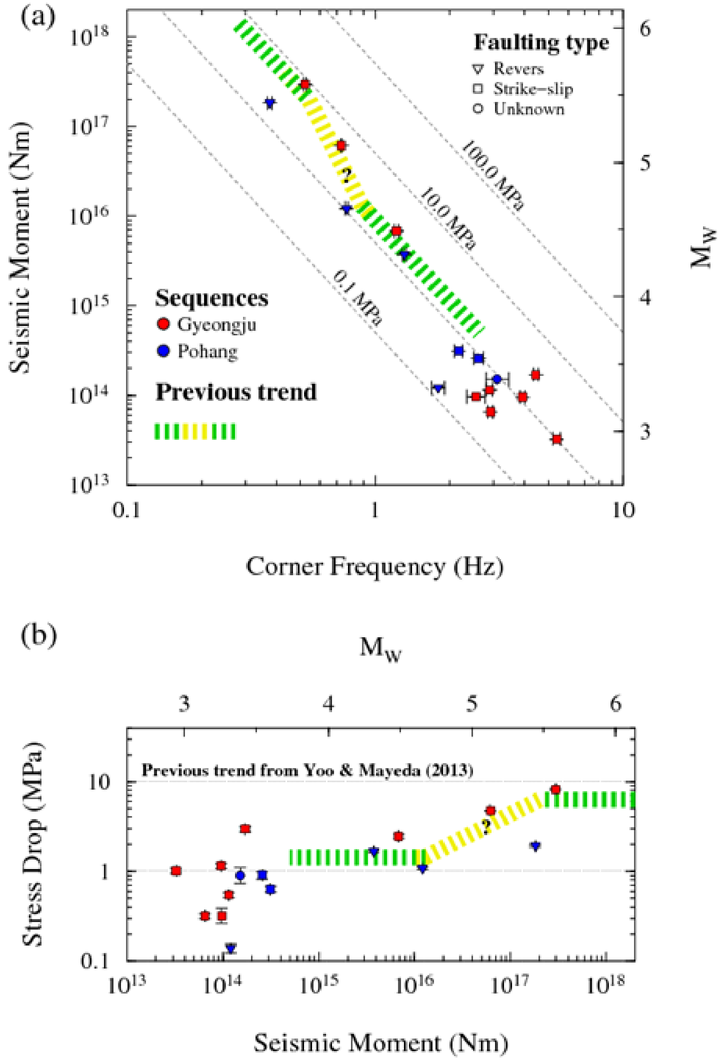

Figure 7. Scaling relations of corner frequency and stress drop versus seismic moment for two earthquake sequences. (a) Constant Brune (1970; 1971) stress drop trends are represented by grey dotted lines. Black vertical and horizontal lines with the symbols represent one standard deviation. The source scaling trend of the Gyeongju sequence follows well with the previously reported trend (thick dotted lines) of coda-based source studies. Both source scaling trends cannot be explained by a constant stress drop model.

Chapter 4.

Conclusions

We analyzed stress drop scaling of two moderate earthquake sequences that occurred in the same tectonic regime. Stress drop seems to increase with increasing magnitude in both sequences. It is interpreted as the result that cannot be explained by the classic self-similar model with constant stress drop (Aki, 1967). The scaling of the GJ sequence is similar to the results of other earthquake sequences studied using similar coda-based methods (Mayeda and Malagnini, 2009; Malagnini *et al.*, 2010; Yoo *et al.*, 2010; Yoo and Mayeda, 2013). The characteristic feature is that stress drop rapidly increases with M_w in a range between M_w 4.5 and 5.5. This rapid increase in stress drop is not found in the PH sequence. On average, stress drops of the PH sequence are lower than those of the GJ sequence. Stress drops of PH02 and PH01 are much smaller than those of events with similar magnitudes in the GJ sequence. Considering previous studies of factors controlling stress drop, it is likely that differences in focal depth between the two sequences caused differences in stress drop. However, difference in focal depth does not explain the particularly low stress drops for two earthquakes in the PH sequence, because all PH events occurred at similar depth. Although further analysis is required to resolve this issue, observations made in this study lead us to the conclusion that we cannot completely rule out the possibility that fluid injection caused lower stress drops for two PH events.

References

Aki, K. (1967). Scaling law of seismic spectrum, *J. Geophys. Res.* **72**(4) 1217-1231, doi: 10.1029/JZ072i004p01217.

Allmann, B. P., and P. M. Shearer (2009). Global variations of stress drop for moderate to large earthquakes, *J. Geophys. Res. Solid Earth* **114**(B1) B01310, doi: 10.1029/2008JB005821.

Bodin, L., and S. I. Gass (2003). On teaching the analytic hierarchy process, *Comput. Oper. Res.* **30**(10) 1487-1497, doi: 10.1016/S0305-0548(02)00188-0.

Boyd, O. S., D. E. McNamara, S. Hartzell, and G. Choy (2017). Influence of lithostatic stress on earthquake stress drops in North America, *Bull. Seismol. Soc. Am.* **107**(2) 856-868, doi: 10.1785/0120160219.

Brune, J. N. (1970). Tectonic stress and the spectra of seismic shear waves from earthquakes, *J. Geophys. Res.* **75**(26) 4997-5009, doi: 10.1029/JB075i026p04997.

Brune, J. N. (1971). Correction to “Tectonic stress and the spectra of seismic shear waves from earthquakes,” *J. Geophys. Res.* **76**(20) 5002, doi: 10.1029/JB076i020p05002.

Ellsworth, W. L., D. Giardini, J. Townend, S. Ge, and T. Shimamoto (2019). Triggering of the Pohang, Korea, Earthquake (M_w 5.5) by enhanced geothermal system stimulation, *Seismol. Res. Lett.* **90**(5) 1844-1858, doi: 10.1785/0220190102.

Eshelby, J. D. (1957). The determination of the elastic field of an ellipsoidal inclusion, and related problems, *Proc. Roy. Soc. Lond. Math. Phys. Sci.* **241**(1226) 376-396, doi: 10.1098/rspa.1957.0133.

Grigoli, F., S. Cesca, A. P. Rinaldi, A. Manconi, J. A. López-Comino, J. F. Clinton, R. Westaway, C. Cauzzi, T. Dahm, and S. Wiemer (2018). The November 2017 M_w 5.5 Pohang earthquake: A possible case of induced seismicity in South Korea, *Science* **360**(6392) 1003-1006, doi: 10.1126/science.aat2010.

Hastings, W. K. (1970). Monte Carlo sampling methods using Markov chains and their applications, *Biometrika* **57**(1) 97–109, doi: 0.2307/2334940.

Hough, S. E. (2014). Shaking from injection-induced earthquakes in the central and eastern United States, *Bull. Seismol. Soc. Am.* **104**(5) 2619-2626, doi: 10.1785/0120140099.

Huang, Y., W. L. Ellsworth, and G. C. Beroza (2017). Stress drops of induced and tectonic earthquakes in the central United States are indistinguishable, *Sci. Adv.* **3**(8) e1700772, doi: 10.1126/sciadv.1700772.

Kim, K. H., J. H. Ree, Y. Kim, S. Kim, S. Y. Kang, and W. Seo (2018). Assessing whether the 2017 M_w 5.4 Pohang earthquake in South Korea was an induced event, *Science* **360**(6392) 1007-1009, doi: 10.1126/science.aat6081.

Kim, S., J. Dettmer, J. Rhie, and H. Tkalčić (2016). Highly efficient Bayesian joint inversion for receiver-based data and its application to lithospheric structure beneath the southern Korean Peninsula, *Geophys. J. Int.* **206**(1) 328-344, doi: 10.1093/gji/ggw149.

Lee, K.-K., W. L. Ellsworth, D. Giardini, J. Townend, S. Ge, T. Shimamoto, I.-W. Yeo, T.-S. Kang, J. Rhie, D.-H. Sheen, C. Chang, J.-U. Woo, and C. Langenbruch (2019). Managing injection-induced seismic risks, *Science* **364**(6442) 730-732, doi: 10.1126/science.aax1878.

Malagnini, L., S. Nielsen, K. Mayeda, and E. Boschi (2010). Energy radiation from intermediate- to large-magnitude earthquakes: Implications for dynamic fault weakening, *J. Geophys. Res. Solid Earth* **115**(B6) B06319, doi: 10.1029/2009JB006786.

Mayeda, K., A. Hofstetter, J. L. O'Boyle, and W. R. Walter (2003). Stable and transportable regional magnitudes based on coda-derived moment-rate spectra, *Bull. Seismol. Soc. Am.* **93**(1) 224-239, doi: 10.1785/0120020020.

Mayeda, K., L. Malagnini, and W. R. Walter (2007). A new spectral ratio method using narrow band coda envelopes: Evidence for non-self-similarity in the Hector Mine sequence, *Geophys. Res. Lett.* **34**(11) L11303, doi: 10.1029/2007GL030041.

Mayeda, K., and L. Malagnini (2009). Apparent stress and corner frequency variations in the 1999 Taiwan (Chi-Chi) sequence: Evidence for a step-wise increase at M_w～5.5, *Geophys. Res. Lett.* **36**(10) L10308, doi: 10.1029/2009GL037421.

McGarr, A. (1984). Scaling of ground motion parameters, state of stress, and focal depth, *J. Geophys. Res. Solid Earth* **89**(B8) 6969-6979, doi: 10.1029/JB089iB08p06969.

McGarr, A., and J. B. Fletcher (2002). Mapping apparent stress and energy radiation over fault zones of major earthquakes, *Bull. Seismol. Soc. Am.* **92**(5) 1633-1646, doi: 10.1785/0120010129.

Metropolis, N., A. W. Rosenbluth, M. N. Rosenbluth, and A. H. Teller (1953). Equation of state calculations by fast computing machines, *J. Chem. Phys.* **21**(6) 1087-1092, doi: 10.1063/1.1699114.

Oth, A. (2013). On the characteristics of earthquake stress release variations in Japan. *Earth Planet. Sci. Lett.* **377-378** 132-141, doi: 10.1016/j.epsl.2013.06.037.

Sokos, E. N., and J. Zahradnik (2008). ISOLA a Fortran code and a Matlab GUI to perform multiple-point source inversion of seismic data, *Comput. Geosci.* **34**(8) 967-977, doi: 0.1016/j.cageo.2007.07.005.

Son, M., C. S. Cho, J. S. Shin, H.-M. Rhee, and D.-H. Sheen (2018). Spatiotemporal distribution of events during the first three months of the 2016 Gyeongju, Korea, earthquake sequence, *Bull. Seismol. Soc. Am.* **108**(1) 210-217, doi: 10.1785/0120170107.

Song, S. G., and H. Lee (2019). Static slip model of the 2017 M_w 5.4 Pohang, South Korea, earthquake constrained by the InSAR data, *Seismol. Res. Lett.* **90**(1) 140-148, doi: 10.1785/0220180156.

Sumy, D. F., C. J. Neighbors, E. S. Cochran, and K. M. Keranen (2017). Low stress drops observed for aftershocks of the 2011 M_w 5.7 Prague, Oklahoma, earthquake, *J. Geophys. Res. Solid Earth* **122**(5) 3813-3834, doi: 10.1002/2016JB013153.

Uchide, T., and S. G. Song (2018). Fault rupture model of the 2016 Gyeongju, South Korea, earthquake and its implication for the underground fault system, *Geophys. Res. Lett.* **45**(5) 2257-2264, doi: 10.1002/2017GL076960.

Vackář, J., J. Burjánek, F. Gallovič, J. Zahradník, and J. Clinton (2017). Bayesian ISOLA: New tool for automated centroid moment tensor inversion, *Geophys. J. Int.* **210**(2) 693-705, doi: 10.1093/gji/ggx158.

Woo, J.-U., M. Kim, D.-H. Sheen, T.-S. Kang, J. Rhie, F. Grigoli, W. L. Ellsworth, and D. Giardini (2019a). An in-depth seismological analysis revealing a causal link between the 2017 M_w 5.5 Pohang earthquake and EGS project, *J. Geophys. Res. Solid Earth* in press, doi: 10.1029/2019JB018368.

Woo, J.-U., J. Rhie, S. Kim, T.-S. Kang, K.-H. Kim, and Y. Kim (2019b). The 2016 Gyeongju earthquake sequence revisited: aftershock interactions within a complex fault system, *Geophys. J. Int.* **217**(1) 58-74, doi: 10.1093/gji/ggz009.

Wu, Q., M. Chapman, and X. Chen (2018). Stress-drop variations of induced earthquakes in Oklahoma, *Bull. Seismol. Soc. Am.* **108**(3A) 1107-1123, doi: 10.1785/0120170335.

Yoo, S.-H. and K. Mayeda (2013). Validation of non-self-similar source scaling using ground motions from the 2008 Wells, Nevada, earthquake sequence, *Bull. Seismol. Soc. Am.* **103**(4) 2508-2519, doi: 10.1785/0120120327.

Yoo, S.-H., J. Rhie, H. Choi, and K. Mayeda (2010). Evidence for non-self-similarity and transitional increment of scaled energy in the 2005 west off Fukuoka seismic sequence, *J. Geophys. Res. Solid Earth* **115**(B8) B08308, doi: 10.1029/2009JB007169.

Yoo, S.-H., J. Rhie, H. Choi, and K. Mayeda (2011). Coda-derived source parameters of earthquakes and their scaling relationships in the Korean Peninsula, *Bull. Seismol. Soc. Am.* **101**(5) 2388-2398, doi: 10.1785/0120100318.

Abstract in Korean

규모 5.0 이상인 2016 경주와 2017 포항 지진이 한반도 남동쪽에서 발생해 진앙지 부근에 피해를 야기했다. 우리는 코다파를 기초로 한 방법과 베이지안 역산법을 이용해서 두 지진 시퀀스의 응력 강하 스케일링을 분석했다. 2016 경주 지진 시퀀스는 일반적인 자연 지진이었지만, 2017 포항 지진 시퀀스는 EGS (Enhanced Geothermal System) 개발을 위한 유체 주입 활동과 관련되어 발생된 지진이라고 여겨진다. 두 시퀀스들이 같은 지질학적 위치에서 발생하였기 때문에 우리 연구에서 자연 지진 시퀀스와 유체 주입에 영향을 받은 지진 시퀀스 사이 응력 강하 스케일링을 서로 비교해볼 수 있는 좋은 기회를 제공한다. 우리의 계산 결과에서 포항 시퀀스의 지진들이 가지는 응력 강하 값이 비슷한 규모에서의 경주 시퀀스의 지진들 보다 더 낮은 응력 강하 값을 가지는 것을 발견했다. 이 현상이 두 시퀀스 사이에 큰 깊이 차이 때문인 것처럼 보이지만, 유체 주입에 의해 응력 강하 값이 줄었을 것이라는 가능성도 배제할 수 없다.

주요 단어: 코다 스펙트럼 비. 코다 소스 계산, 모서리 주파수, 응력 강하, 소스 스케일링

학생 번호: 2017-24073